Architectural Engineering of Rod–Coil Compatibilizers for Producing Mechanically and Thermally Stable Polymer Solar Cells

Hyeong Jun Kim,[†] Jae-Han Kim,[‡] Ji-Ho Ryu,[§] Youngkwon Kim,[†] Hyunbum Kang,[†] Won Bo Lee,[§] Taek-Soo Kim,[*,‡] and Bumjoon J. Kim[*,†]

[†]Department of Chemical and Biomolecular Engineering, Korea Advanced Institute of Science and Technology (KAIST), Daejeon 305-701, Korea, [‡]Department of Mechanical Engineering, Korea Advanced Institute of Science and Technology (KAIST), Daejeon 305-701, Korea, and [§]Department of Chemical and Biomolecular Engineering, Sogang University, Seoul 121-742, Korea

ABSTRACT While most high-efficiency polymer solar cells (PSCs) are made of bulk heterojunction (BHJ) blends of conjugated polymers and fullerene derivatives, they have a significant morphological instability issue against mechanical and thermal stress. Herein, we developed an architecturally engineered compatibilizer, poly(3-hexylthiophene)-*graft*-poly(2-vinylpyridine) (P3HT-*g*-P2VP), that effectively modifies the sharp interface of a BHJ layer composed of a P3HT donor and various fullerene acceptors, resulting in a dramatic enhancement of mechanical and thermal stabilities. We directly measured the mechanical properties of active layer thin films without a supporting substrate by floating a thin film on water, and the enhancement of mechanical stability without loss of the electronic functions of PSCs was successfully demonstrated. Supramolecular interactions between the P2VP of the P3HT-*g*-P2VP polymers and the fullerenes generated their universal use as compatibilizers regardless of the type of fullerene acceptors, including mono- and bis-adduct fullerenes, while maintaining their high device efficiency. Most importantly, the P3HT-*g*-P2VP copolymer had better compatibilizing efficiency than linear type P3HT-*b*-P2VP with much enhanced mechanical and thermal stabilities. The graft architecture promotes preferential segregation at the interface, resulting in broader interfacial width and lower interfacial tension as supported by molecular dynamics simulations.

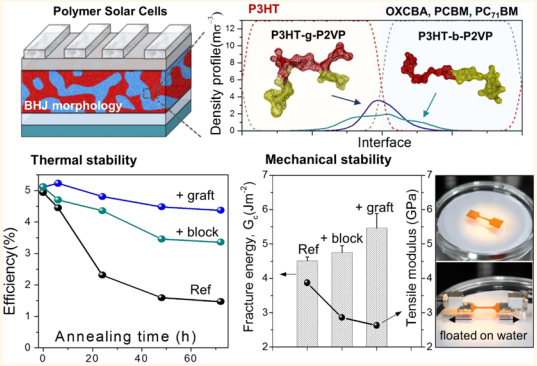

KEYWORDS: thermal and mechanical stability of polymer solar cell · rod–coil copolymer · graft and block architecture · universal compatibilizer · coarse-grained molecular dynamics simulations

A significant amount of academic and industrial efforts have been dedicated to resolving scientific and technological issues in the development of efficient polymer solar cells (PSCs) and their practical implementations.[1−6] One of the most successful advances was achieved with the advent of bulk-heterojunction (BHJ) morphology that forms a large donor (D)–acceptor (A) interface in close proximity to the region of exciton diffusion and dissociation (5–10 nm) while maintaining the percolating pathway for charge transport to the electrode.[7−9] Currently, BHJ blends comprising π-conjugated polymers and fullerene derivatives dominate the field of high-efficiency PSCs, and the highest power conversion efficiency (PCE) is now approaching about 10%.[10,11]

Despite such success, BHJ blends of polymer/fullerene have significant morphological instability issues originating from strong immiscibility between polymers and fullerenes, resulting in the formation of weak D/A junctions that have very sharp interfaces with poor adhesion. The optimized BHJ morphology is typically obtained from a kinetic trap process during the solution processing of two immiscible components.[12,13] Therefore, the BHJ morphology under nonequilibrium status tends to shift toward macrophase separation to reduce the thermodynamically

* Address correspondence to bumjoonkim@kaist.ac.kr, tskim1@kaist.ac.kr.

Received for review July 12, 2014 and accepted September 25, 2014.

Published online September 25, 2014
10.1021/nn503823z

unstable interfaces as subsequent heat exposure upon extended device operation.[14−16] Furthermore, the sharp and unstable interfaces between D/A junctions cause mechanical fragility in the active layer within the relatively low value of cohesion and ductility.[17,18] For example, when phenyl-C_{61}-butyric acid methyl ester (PCBM) is added to poly(3-hexylthiophene) (P3HT), the blended film becomes stiffer and more brittle with a higher value of tensile modulus than that of the pure polymer film. As a result, a 1:1 mixture of P3HT/PCBM fractured at strains of only about 2% on a stretchable substrate.[19,20] Such progressive phase separation and mechanically fragile properties of BHJs ultimately lead to significant loss of the performance and reliability of PSCs during subsequent operation. Therefore, D/A interfaces in BHJ blends must be modified to improve the morphological stability against phase separation and mechanical failure. In particular, considering all of the potential applications of the PSCs as printable and portable devices on flexible substrates, the importance of enhancing the mechanical properties of the PSCs will be greatly amplified.[10,21]

The sharp interface between two immiscible phases can be modified by the addition of compatibilizers because unfavorable interactions can be alleviated by the accumulation of compatibilizers at the interface.[22−25] The first example of compatibilizers in the BHJ PSCs was demonstrated by Frechet *et al.*[26] Block copolymer type compatibilizers were designed to have two different blocks of P3HT and fullerene, and the block copolymer retards phase separation of BHJ PSCs under long-term heat exposure. After this work, various types of compatibilizers including copolymers,[27−31] small molecules,[32−34] end-capped polymers,[35] and *in situ* compatibilizers[36] have been reported with their effects on the thermal stability of the PSCs. However, while most of the compatibilizers mentioned above contain covalently linked fullerene molecules to generate preferential enthalpic interactions with the fullerene acceptor phase of the BHJ active layer, the synthesis of such compatibilizers is not trivial; multiple postpolymerization steps are often required, and low solubility of the fullerene causes low yield of reactions.[26−29] More importantly, the addition of covalent linkages to fullerene molecules causes significant changes of their intrinsic electrical properties including energy levels and electron mobilities, which are the critical factors in affecting the efficiency of the PSCs.[37−39] In particular, the development of appropriate compatibilizers for bis-adduct fullerene based BHJ systems still remains a challenge, while the bis-adduct fullerenes have been considered as very promising acceptors for amplifying open-circuit voltage and consequently PCE due to their higher lowest unoccupied molecular orbital (LUMO) energy levels than singly functionalized PCBM.[40−43] The use of noncovalent interactions would be a promising way to overcome these drawbacks; for example, electron-rich polymers such as poly(vinylpyridine) are known to have strong supramolecular interactions with electron-deficient fullerene molecules.[44−46] Although some studies have shown the possibility of using noncovalent supramolecular interactions to design active layers[47] and structuring agents[48,49] in PSCs, a compatibilizer based on supramolecular interaction for enhancing the morphological stability of PSCs has not been demonstrated. None of works have studied the effect of compatibilizers on the mechanical properties of PSCs despite their great importance for the robust operation and reliability of PSCs.

Herein, we developed a new architectural design for effective compatibilizers and demonstrated their use for the stable operation of a polymer/fullerene BHJ against thermal stress and mechanical failure. We utilized P3HT-*graft*-poly(2-vinylpyridine) (P3HT-*g*-P2VP) copolymers[50] as compatibilizers, which could effectively modify the sharp interface of the BHJ comprising the P3HT donor and various fullerene acceptors (*o*-xylenyl C_{60} bis-adduct (OXCBA), PCBM, and $PC_{71}BM$), resulting in dramatic enhancement of thermal and mechanical stabilities. The supramolecular interaction between the P2VP block of P3HT-*g*-P2VP polymers and the fullerenes resulted in the enhancement of thermal and mechanical stabilities for all different PSC systems even including bis-adduct-type fullerene while maintaining a PCE value greater than 5%. To demonstrate the effectiveness of our new P3HT-*g*-P2VP compatibilizers, we also synthesized P3HT-*block*-poly(2-vinylpyridine) (P3HT-*b*-P2VP) copolymers that had the same P3HT block length and volume fractions. It was evident from the results of the thermal and mechanical properties of the PSCs that the graft architectured P3HT-*g*-P2VP copolymers had much better compatibilizing power than linear-type P3HT-*b*-P2VP copolymers. The effectiveness of the graft architecture was further demonstrated by coarse-grained molecular dynamics simulations to describe the effects of molecular configurations on interfacial width and tension for both P3HT-*g*-P2VP and P3HT-*b*-P2VP polymers at the D/A interface.

RESULTS AND DISCUSSION

P3HT-*g*-P2VP and P3HT-*b*-P2VP rod−coil copolymers were synthesized using a microwave-assisted click reaction between azide functional groups in P3HT polymers and alkyne-terminated P2VP polymers according to the modified literature procedure[50] (Scheme 1). For producing graft or block architecture, two different azide-functionalized P3HTs were prepared *via* Grignard metathesis (GRIM) polymerization. One has azide groups at the end of an alkyl chain of 3-hexylthiophene units (3-(azidohexyl)thiophene) in the polymers (P3HT-alkyl-azide), and the other has only one azide group at the end of the polymer

chain (P3HT-end-azide) (Schemes S1 and S2). The polymerization conditions including reaction time and concentration were controlled to produce a similar molecular weight (M_n) of both P3HT polymers (P3HT-alkyl-azide M_n = 6.8 kg/mol, P3HT-end-azide M_n = 6.4 kg/mol) with a narrow polydispersity index (PDI) value. Detailed preparation of P3HT-alkyl-azide followed a previously described method.[36] The composition of 3-(azidohexyl)thiophene monomers was confirmed by ^{1}H NMR and controlled to be 5 mol %, of which one P3HT-alkyl-azide chain contains an average number of two azide units. For the synthesis of P3HT-end-azide polymers, a vinyl end-capped P3HT chain was polymerized first according to the route reported by McCullough *et al.*,[51] and the vinyl group at the end of the P3HT chain was converted into a hydroxyl group and then into a azide group.[52] The vinyl end-capped P3HT polymers contained very homogeneous Br/vinyl end-groups, as evidenced by MADLI-TOF (Figure S2). The substitution reaction of vinyl groups was successfully performed as monitored by ^{1}H NMR (Figures S3 and S4) and Fourier transform infrared (FT-IR) (Figure S5). In the meantime, a series of P2VP-alkynes with different $M_{n,P2VP}$ values were polymerized by using an alkyne-terminated reversible addition–fragmentation transfer (RAFT) chain transfer agent.[38] The resulting P2VP-alkyne polymers were then coupled with two different P3HT-alkyl-azide and P3HT-end-azide polymers *via* the microwave-assisted click reaction to produce a series of P3HT-*g*-P2VP and P3HT-*b*-P2VP copolymers, respectively. It should be noted that both P3HT-*g*-P2VP and P3HT-*b*-P2VP polymers have two different well-matched volume fractions of P3HT (f_{P3HT}) of approximately 0.45 and 0.35, respectively. These are labeled P3HT-*g*-P2VP(0.43), P3HT-*g*-P2VP(0.34), P3HT-*b*-P2VP(0.47), and P3HT-*b*-P2VP(0.36). The M_n and PDI values of P3HT-alkyl-azide and P3HT-end-azide were obtained by size exclusion chromatography (SEC) calibrated with PS standards, and then the f_{P3HT} values for four different copolymers were calculated from ^{1}H NMR (Figures S1 and S6). Table 1 summarizes the characteristics of the P3HT-*g*-P2VP and P3HT-*b*-P2VP copolymers. Details of the synthesis and characterizations are described in the Supporting Information.

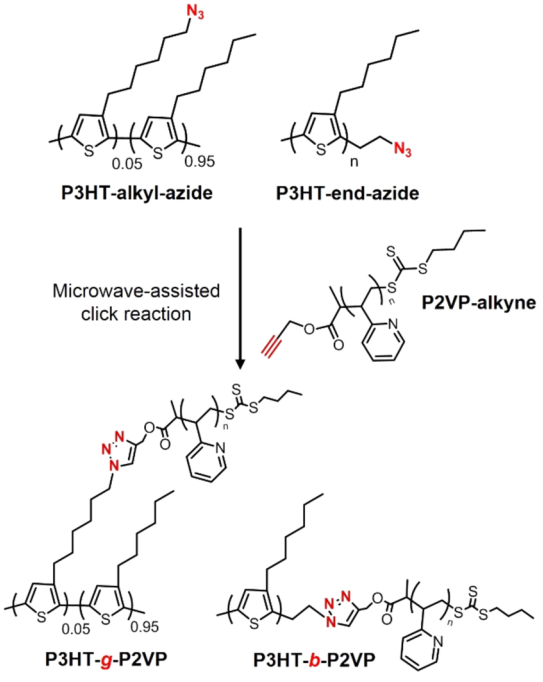

Scheme 1. Synthesis of the P3HT-*g*-P2VP and P3HT-*b*-P2VP copolymers *via* microwave-assisted azide–alkyne click reaction. The P3HT-*g*-P2VP and P3HT-*b*-P2VP copolymers have the similar volume fractions and block lengths of the P3HT.

In order to explore the potential of P3HT-*g*-P2VP and P3HT-*b*-P2VP rod–coil copolymers as compatilizers for the PSCs, they were incorporated as additives into the BHJ PSC devices consisting of P3HT and various fullerene derivatives including OXCBA, PCBM, and $PC_{71}BM$ (Figure 1). The inverted-type PSC has many advantages over the conventional-type in terms of ambient device stability and suitability for use in large-area solution processing techniques.[53] Therefore, the inverted PSCs with ITO/ZnO/P3HT:(OXCBA, PCBM, or $PC_{71}BM$)/PEDOT:PSS/Ag geometry were fabricated in the presence of either P3HT-*g*-P2VP or P3HT-*b*-P2VP.

Figure 2 shows the performances of P3HT/OXCBA BHJ devices without any compatibilizers and with 5 wt % of P3HT-*g*-P2VP(0.43), P3HT-*g*-P2VP(0.34), P3HT-*b*-P2VP(0.47), and P3HT-*b*-P2VP(0.36) copolymers, respectively, as a function of annealing time at 150 °C. We have chosen the P3HT/OXCBA pair as a model system because P3HT/OXCBA is one of the most efficient P3HT-based PSCs with nearly 50% higher PCE (PCE ≈ 5%) than P3HT/PCBM.[39,42,54] The weight ratio of rod–coil copolymers to P3HT in the active layer varied from 0% to 15%, and the optimized weight ratio was found to be 5% for all of different rod–coil copolymers,

TABLE 1. Characteristics of Polymers Used in the Study

rod–coil copolymers	type	$M_{n,P3HT}$[b] [g/mol]	P3HT PDI[b]	$M_{n,P2VP}$[c] [g/mol]	P2VP PDI[b]	f_{P3HT}[d]
P3HT-*g*-P2VP(0.43)	graft (5 mol %)[a]	6.8 K	1.18	4.6 K	1.13	0.43
P3HT-*g*-P2VP(0.34)				7.1 K	1.10	0.34
P3HT-*b*-P2VP(0.47)	block	6.4 K	1.09	6.9 K	1.10	0.47
P3HT-*b*-P2VP(0.36)				11.7 K	1.14	0.36

[a] Determined from the ^{1}H NMR spectra of P3HT-alkyl-azide. [b] Determined from SEC measurements. [c] Determined from ^{1}H NMR spectra of copolymers. [d] Calculated based on the integration of ^{1}H NMR with densities of 1.10 g cm^{-3} for P3HT and 1.14 g cm^{-3} for P2VP.

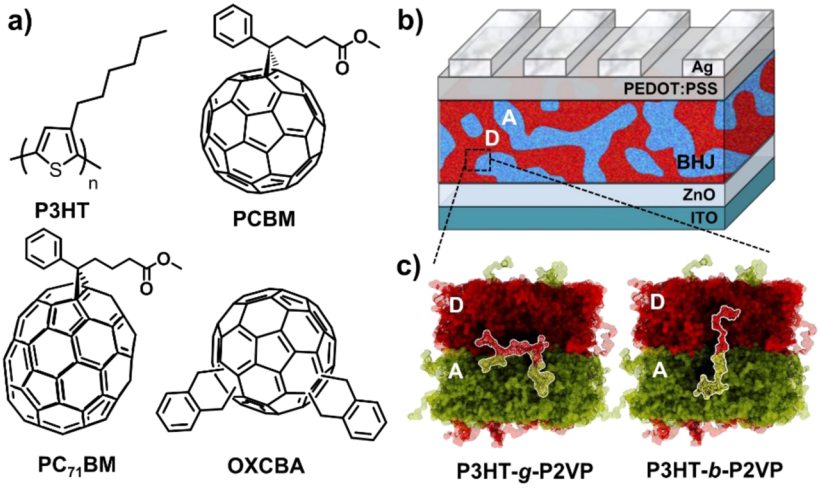

Figure 1. (a) Chemical structures of the conjugated polymer electron donor (P3HT) and various fullerene derivative electron acceptors (OXCBA, PCBM, and $PC_{71}BM$) used in this study. (b) Device architecture of inverted-type PSC applied in this study, and (c) the predicted molecular configurations of graft and block copolymers at the interface between the D/A phases of the BHJ active layer.

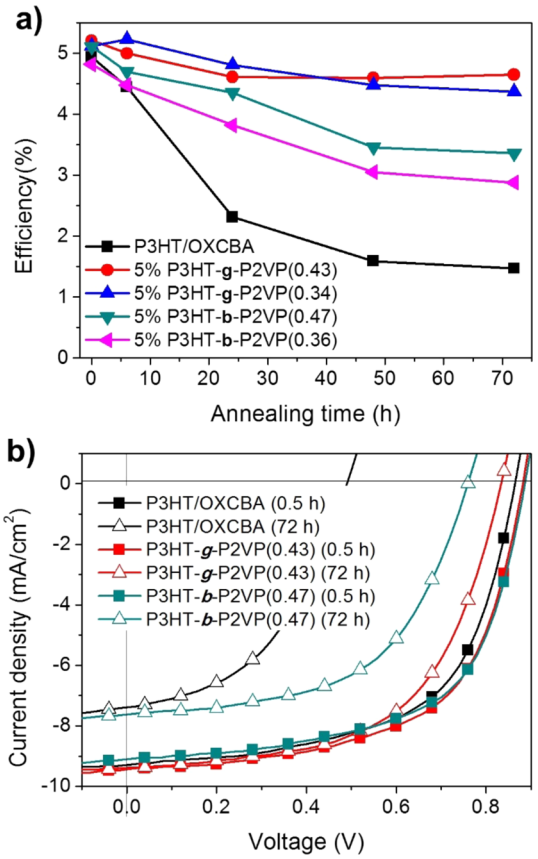

Figure 2. (a) Efficiencies of P3HT/OXCBA devices containing 5 wt % of P3HT-*g*-P2VP(0.43), P3HT-*g*-P2VP(0.34), P3HT-*b*-P2VP(0.47), and P3HT-*b*-P2VP(0.36) copolymers at different times of thermal annealing at 150 °C. (b) Current−voltage curves of the representative devices made of P3HT/OXCBA, +5% P3HT-*g*-P2VP(0.43), and +5% P3HT-*b*-P2VP(0.47) with initial (0.5 h) and long-term (72 h) thermal annealing.

producing the maximal PCE values (Figure S7 and Table S1). Our rod−coil compatibilizers for the P3HT/OXCBA devices produced similar or even higher PCE values than those of the reference device, whereas no successful example of compatibilizers for the bis-adduct fullerene based PSCs has been demonstrated (Table 2). This result is mainly due to our molecular design of P3HT-*g*-P2VP copolymers that utilize the noncovalent, supramolecular interaction with fullerenes, which does not affect the electrical properties of OXCBA. All of the rod−coil copolymers induced greatly enhanced thermal stabilities in the PSC devices, which is in stark contrast to that of the reference device without compatibilizers (Table 2). It is remarkable to note that the PSC device with the addition of P3HT-*g*-P2VP(0.43) by 5 wt % had superior thermal stability, producing a PCE of higher than 4.65% even after 72 h of annealing at 150 °C. To the best of our knowledge, this represents the most efficient and thermally stable P3HT-based BHJ device. In contrast, the device performance of the pristine P3HT/OXCBA blends decreased to a third of its initial efficiency value (PCE = 1.61%) after the same thermal treatment. This dramatic contrast in thermal stability shows the benefits of the P3HT-*g*-P2VP(0.43) compatibilizers for stable PSC

TABLE 2. Photovoltaic Parameters of P3HT/OXCBA Devices with Prolongated Thermal Annealing at 150 °C

	annealing time (h)	V_{oc} (V)	J_{sc} (mA/cm^2)	FF	PCE (%)
P3HT/OXCBA	0.5	0.87	9.30	0.61	4.94
	72	0.49	7.48	0.44	1.61
P3HT-*g*-P2VP(0.43)	0.5	0.89	9.28	0.63	5.21
	72	0.84	9.20	0.60	4.65
P3HT-*g*-P2VP(0.34)	0.5	0.88	9.19	0.64	5.12
	72	0.81	8.93	0.60	4.37
P3HT-*b*-P2VP(0.47)	0.5	0.89	9.30	0.61	5.11
	72	0.76	7.64	0.58	3.36
P3HT-*b*-P2VP(0.36)	0.5	0.89	8.50	0.63	4.82
	72	0.77	7.17	0.52	2.88

operation. It is interesting to note that the devices containing the graft copolymer compatibilizers exhibited a much higher thermal stability compared to the devices with block copolymer compatibilizers. For example, after the same thermal treatment (72 h at 150 °C), the device that contained 5 wt % of P3HT-*g*-P2VP(0.34) shows a much higher efficiency (PCE = 4.37%) than the devices with 5% P3HT-*b*-P2VP(0.47) (PCE = 3.36%) and P3HT-*b*-P2VP(0.36) copolymers (PCE = 2.88%), while P3HT-*g*-P2VP(0.34) has a very similar P2VP block length P3HT-*b*-P2VP(0.47) and a similar f_{P3HT} value to P3HT-*b*-P2VP(0.36). In order to enhance the versatility of the P3HT-*g*-P2VP compatibilizers for other PSC systems, our rod−coil copolymers were further applied to other BHJ PSCs systems such as P3HT/PCBM (Figure S8 and Table S2) and P3HT/$PC_{71}BM$ (Figure S9 and Table S3). The devices containing the P3HT-*g*-P2VP copolymers exhibited much higher thermal stabilities than those with the P3HT-*b*-P2VP copolymers, which showed consistent trends with those described in the P3HT/OXCBA system. These results clearly demonstrated that graft architecture is much more favorable for modifying the sharp interface between P3HT/OXCBA and for producing highly thermally stable BHJ PSCs. Also, universal compatibilization of P3HT/fullerene BHJ PSCs can be successfully achieved by utilizing our copolymers regardless of the type of fullerene acceptors.

The effect of the P3HT-*g*-P2VP compatibilizers on the thermal stability of the PSC performance can be visualized by direct examination of the morphology of the active layer through transmission electron microscopy (TEM) (Figure 3). The TEM samples were prepared identically to the optimized device condition according to the previously reported method.[55,56] After 30 min of thermal annealing at 150 °C, the P3HT/OXCBA film exhibited well-developed interpenetrating networks consisting of long P3HT fibrils, which provide maximum interfacial area for charge generation and efficient charge transport pathway. However, progressive and severe phase separation occurred in the presence of clusters of fullerene molecules with a length scale of 20−50 nm when the prolongated thermal annealing was applied (Figure 3 and Figure S10). The size of the fullerene aggregates, however, was much smaller compared to those of PCBM or other monoadduct fullerene derivative. Fullerene bis-adducts are known to have relatively low crystallinity and thus a weaker trend for crystallization because the presence of their regioisomers and second substituent hinders the close contact of fullerene cores from forming large clusters.[57,58] In striking contrast, the morphologies of BHJ films that contained 5 wt % of P3HT-*g*-P2VP and P3HT-*b*-P2VP remain almost unchanged, as shown in Figure 3c and d after 24 h of annealing at 150 °C. The same trend of compatibilizing effects by P3HT-*g*-P2VP polymers was clearly observed for other PSC systems of P3HT/PCBM.

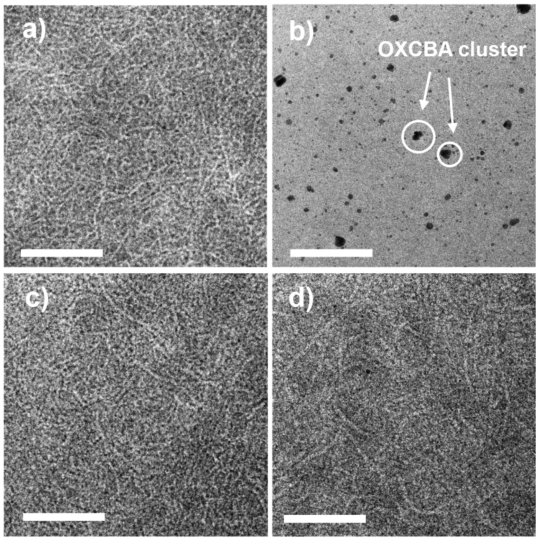

Figure 3. TEM images of P3HT/OXCBA films after (a) 0.5 h of annealing and (b) 24 h of annealing at 150 °C. OXCBA clusters were found after 24 h of annealing. In contrast, the devices that contained 5 wt % of (c) P3HT-*g*-P2VP(0.43) and (d) P3HT-*b*-P2VP(0.47) maintained their morphology without any aggregation of fullerenes after 24 h of annealing at 150 °C. Scale bars are 200 nm.

Both the optical microscopy and grazing incidence wide-angle X-ray scattering results confirmed that the presence of rod−coil compatibilizers successfully suppressed macrophase separation, thus enabling thermally stable performances of the PSCs (Figures S11 and S12). Although the comparison of the BHJ morphology by TEM did not provide sufficient contrast in the morphologies between the graft and the block copolymer added BHJ layer, this morphological observation strongly demonstrated the excellent ability of P3HT-*g*-P2VP and P3HT-*b*-P2VP compatibilizers for reducing the interfacial tension and for preventing the morphologies from undergoing phase separation.

For an in-depth study to elucidate the effect of our rod−coil compatibilizers on the mechanical properties of BHJ active layers, we measured both fracture energy and elastic modulus of the BHJ layer, which represent the mechanical properties in the perpendicular and horizontal directions, respectively. The cohesive fracture energies of both P3HT/PCBM and P3HT/OXCBA in the presence of the compatibilizers were compared using the double cantilever beam (DCB) fracture mechanics testing method (Figure 4a).[59−61] The DCB specimens were prepared with the geometry glass/P3HT:(OXBA or PCBM)/Pt/epoxy/glass. The identical conditions of optimized PSCs were used for the preparation of the active layer, and the sputtered Pt layer was introduced to prevent the diffusion of the epoxy resin. Cohesive failure of the BHJ layer was observed in all the specimens (Figure S13). The critical cohesive fracture energy (G_c) values for P3HT/PCBM BHJ films were measured to be 3.73 ± 0.18 J m^{-2}, which agreed well with the previously reported value for fracture

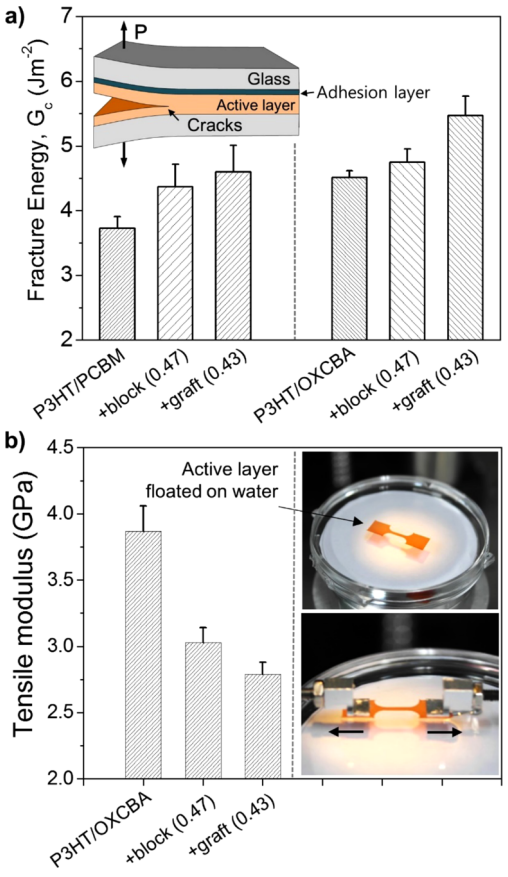

Figure 4. (a) Comparison of internal cohesive fracture energy of the P3HT/PCBM and P3HT/OXCBA BHJ films in the presence of 5% of P3HT-*g*-P2VP(0.43) and P3HT-*b*-P2VP-(0.47). The structure of specimens for the measurement of the cohesive energy of the active layer is illustrated. (b) Tensile modulus of the P3HT/OXCBA films containing 0% or 5% of P3HT-*g*-P2VP(0.43) and P3HT-*b*-P2VP(0.47). The active layer thin films were afloat on the water surface with alignment and grip attachment.

energy of P3HT/PCBM devices prepared under similar conditions.[18,62,63] Interestingly, the G_c values were increased up to 4.42 ± 0.75 and 4.32 ± 0.41 J m^{-2} for the P3HT/PCBM films that contained 5% of P3HT-*g*-P2VP(0.43) and P3HT-*b*-P2VP(0.47) copolymers, respectively. Similar trends were observed for the P3HT/OXCBA system. The P3HT/OXCBA film exhibited a G_c value of 4.51 ± 0.11 J m^{-2}, but the films with 5% of P3HT-*g*-P2VP(0.43) and P3HT-*b*-P2VP(0.47) had much larger G_c values of 5.46 ± 0.42 and 4.75 ± 0.20 J m^{-2}, respectively. Preferential localization of our rod−coil compatibilizers at the D/A interface can increase the entanglement density of the polymer chains across the interface, which lead to increase the energy needed to be broken for cohesive failure of BHJ films. In addition, the covalent joint between P3HT and P2VP blocks of the compatibilizers could enhance the resistance against the crack growth and the debonding between the two phases.

Next, we measured the tensile modulus of BHJ active layers, which are more closely related for the realization of flexible and stretchable PSC applications. Despite such importance, not much work has been done on even basic measurement of the tensile modulus of the active layer in PSCs. Recently, the elastic modulus of thin films of P3HT/PCBM BHJ was measured by utilizing an underlying compliant substrate.[19,64] However, extracting mechanical properties of the active layer from the underlying substrate is challenging because the thickness of the BHJ active layer for efficient PSC is typically less than 200−300 nm, and the adhesion between the thin film and the underlying substrate causes additional difficulty.[20,65] Therefore, we conducted a "pseudo free-standing tensile test",[65] which enables direct measurement of the tensile modulus without specimen damage or substrate effects by utilizing the water surface as the underlying support for free-standing thin films. Figure 4b shows the elastic modulus of the P3HT/OXCBA with 0% or 5% of P3HT-*g*-P2VP(0.43) and P3HT-*b*-P2VP(0.47). The pictures of specimens floating on water are shown in Figure 4b. Specimen gripping was performed by attaching polydimethylsiloxane (PDMS)-coated grips, and tensile test was performed by a linear stage with a strain rate of 6×10^{-5}/s.[65] The Young's modulus of the P3HT/OXCBA film was found to be 3.87 GPa. In contrast, the tensile modulus decreased remarkably to 3.03 and 2.79 GPa, respectively, with the addition of 5% P3HT-*b*-P2VP(0.47) and P3HT-*g*-P2VP(0.43) compatiblizers. It should be noted that this is the first time that the modulus of an active layer of a solar cell was measured directly without a supporting layer. More importantly, the addition of rod−coil compatibilizers, especially with the graft architecture, enhances the fracture energy between two immiscible phases and reduces the tensile modulus without any loss of electronic function of PSCs. The low modulus of the BHJ film allows the PSCs to tolerate mechanical deformations such as bending or stretching without the formation of a crack.[20,66] Mechanical stability experiments consistently lead to the same conclusion that the graft architecture is more efficient as the compatibilizer in the PSCs.

To gain a deeper understanding of interfacial activity differences between P3HT-*g*-P2VP and P3HT-*b*-P2VP compatiblizers, we performed coarse-grained bead-spring (CGBS) molecular dynamics simulation, in which a collection of atoms is mapped into a smaller number of beads. Initially, we constructed an immiscible D/A homopolymer bilayer blend, and then energy minimization and a simulated annealing process were applied to obtain the minimum energy structure. The density profiles of D/A binary blends are shown in Figure S14, and there is a flat and sharp interface between immiscible A and B regions. Into that system, we introduced equal numbers of the simulated P3HT-*g*-P2VP and P3HT-*b*-P2VP copolymers, which have the same molecular shape and length scale as P3HT-*g*-P2VP-(0.43) and P3HT-*b*-P2VP(0.47), respectively. Then, the

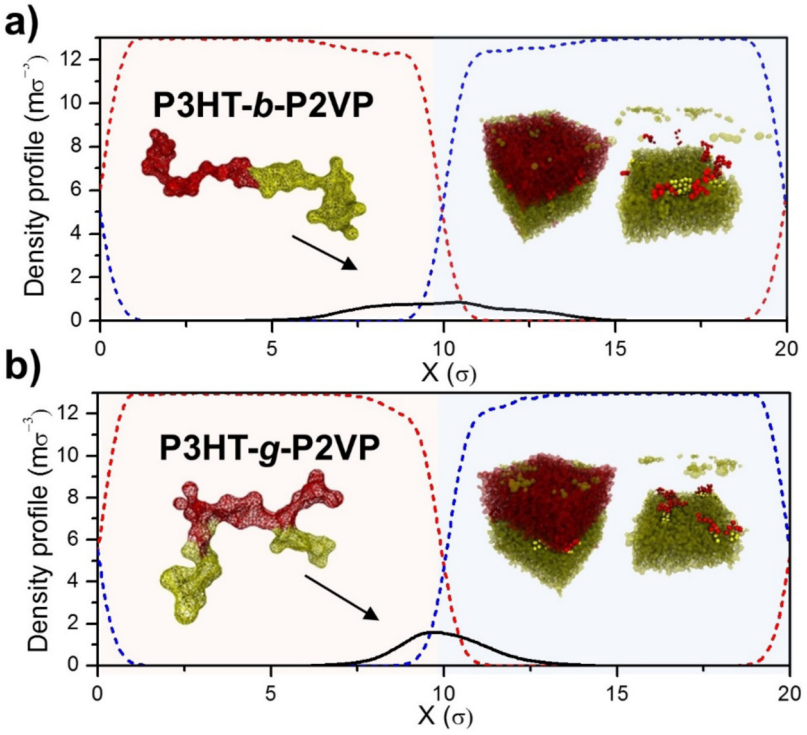

Figure 5. Simulated density profiles of (a) P3HT-*b*-P2VP and (b) P3HT-*g*-P2VP copolymers at the immiscible D/A blends at the minimum energy states. P3HT-*g*-P2VP copolymer has a higher areal chain density at the interface and broader interfacial width compared to linear-type P3HT-*b*-P2VP copolymer.

same energy minimization and simulated annealing steps were applied to the D/A binary blends + (P3HT-*g*-P2VP or P3HT-*b*-P2VP) system. The density profiles of D/A homopolymers and copolymers are shown in Figure 5. P3HT-*g*-P2VP copolymer has a higher areal chain density close to the interface between the D and A phase, whereas the linear-type P3HT-*b*-P2VP copolymer has a broader density distribution. These results indicate that graft architecture has structural advantages for preferential segregation at the interface with a minimum energy state. For a precise comparison of interfacial width changes due to the addition of two different copolymers, interfacial width (δ) is calculated by a previously reported equation.[67,68] The δ is calculated to be 1.033σ for the D/A blend system, and δ was broadened to 1.194σ and 1.272σ with the addition of P3HT-*b*-P2VP and P3HT-*g*-P2VP copolymers, respectively (Table 3). Preferential localization of P3HT-*g*-P2VP copolymers at the interface increases the interfacial width between two immiscible components. Through CGBS simulation, the interfacial tension (γ_s) of the systems, which is the most important parameter for determining the compatibilizing effectiveness of the copolymers and directly related to the tendency for phase separation upon heat exposure, can be further calculated using the modified Irving and Kirkwood equation.[69] The calculated γ_s values are listed in Table 3. The graft copolymers produced the lowest interfacial tension value in the immiscible blend system, which is well matched with the experimental results of P3HT-*g*-P2VP copolymers. The broad interfacial width and low interfacial tension due to the higher preferential segregation of the graft copolymer at the interface induce strong enhancements of the mechanical and thermal stabilities of immiscible binary blends.

TABLE 3. Comparison of the Interfacial Properties of the D/A Blends without and with Rod−Coil Compatibilizers

compatibilizer	interfacial width (δ)	interfacial tension (γ_s)
D/A blends	1.033σ	$0.224\sigma^{-2}k_BT$
P3HT-*b*-P2VP	1.194σ	$0.190\sigma^{-2}k_BT$
P3HT-*g*-P2VP	1.272σ	$0.180\sigma^{-2}k_BT$

CONCLUSIONS

In this work, we demonstrated new architectured P3HT-*g*-P2VP polymers for the use of effective compatbilizers in mechanically and thermally stable PSCs. The addition of P3HT-*g*-P2VP compatibilizer into BHJ PSCs effectively modified the sharp interface between P3HT and fullerene derivatives, resulting in superb thermal and mechanical stabilities without any loss of performance. The P3HT-*g*-P2VP copolymer universally enhanced the stability of BHJ PSCs regardless of the type of fullerene acceptors including bis-adduct fullerenes. The P3HT/OXCBA device with 5% of P3HT-*g*-P2VP exhibited a PCE of over 4.6% even after 72 h annealing at 150 °C, which represents one of

the best thermal stability performances in the PSCs. In addition, the fracture energy of BHJ PSCs was also increased above 20% compared to the reference device. We directly measured the tensile modulus of active layer without the supporting layer and examined the effect of the compatibilizers on the mechanical property of PSCs for the first time. More importantly, graft architecture of copolymers could promote a better compatibilzing effect that leads to higher thermal and mechanical stability compared to P3HT-*b*-P2VP with well-matched volume fraction and block length of P3HT. The effectiveness of graft architecture was well supported by the results from coarse-grained molecular dynamics simulations. Our results provide guidelines for the design of of effective compatibilizers toward thermally and mechanically stable operation of PSCs.

METHODS

Materials. P3HT was obtained from RIEKE Corporation with an approximate M_n of 20 K. PCBM and $PC_{71}BM$ were synthesized by the previously reported procedure.[70] Highly purified OXCBA was synthesized according to our previous paper.[42,54] The detailed synthetic procedures of P3HT-*g*-P2VP and P3HT-*b*-P2VP are described in the Supporting Information

Device Fabrication and Measurement. Indium tin oxide (ITO)-coated glass substrates were subjected to ultrasonication in different solvent systems including acetone, 2% soap in water, deionized water, and then 2-propanol. The ZnO was prepared using a sol−gel procedure, dissolving zinc acetate dihydrate ($Zn(O_2CCH_3)_2 \cdot (H_2O)_2$, 99.9%, 1 g) and ethanolamine ($NH_2C_2H_5OH$, 99.5%, 0.28 g) in anhydrous 2-methoxyethanol (10 mL) under vigorous stirring for more than 24 h to allow the hydrolysis reaction. ZnO thin films with a thickness of ∼40 nm were prepared by spin-coating the sol−gel precursor solution at 4000 rpm on top of the ITO substrate. The films were heated at 200 °C for 1 h in air. After application of the ZnO layer, all subsequent procedures were performed in a glovebox under a N_2 atmosphere. P3HT/PCBM or $PC_{71}BM$ (1:0.67 wt %) and P3HT/OXCBA (1:0.6 wt %) with 60 mg/mL of P3HT concentration were dissolved in ODCB and stirred at 90 °C for more than 24 h. The solutions were passed through a 0.2 μm PTFE syringe filter. Blended solutions (P3HT/(PCBM, $PC_{71}BM$, or OXCBA) + P3HT-*g*-P2VP or + P3HT-*b*-P2VP) were prepared with a final P3HT concentration of 15 mg/mL, and the weight ratio of copolymers with respect to the P3HT was varied from 0% to 15%. Active layer blend solutions were spin-cast onto an ITO/ZnO substrate at 900 rpm for 40 s. PEDOT:PSS (VAITRON AI 4083) was then spin-cast at 4000 rpm on top of the aforementioned layer using X-triton 100 (1−1.5 wt %) as processing additive to form a smooth layer with a thickness of ∼40 nm and then annealed at 120 °C in the glovebox for 10 min. Finally, to complete the devices, the top electrode, 100 nm Ag film, was thermally evaporated under high vacuum (less than 10^{-6} Torr). The active area of the fabricated devices was 0.09 cm^2. The photovoltaic performance of the devices was characterized with a solar simulator (Peccell) with an air mass (AM) 1.5 G filter. The intensity of the solar simulator was carefully calibrated using an AIST-certified silicon photodiode. The current−voltage behavior was measured using a Keithley 2400 SMU.

Double Cantilever Beam Based Adhesion Technique Testing. For DCB specimen preparation, the active layer that has the same condition as the optimized solar cells is first spin-coated on a bare glass substrate. A 50 nm thick Pt layer is deposited by a sputtering process in order to prevent the penetration of epoxy into the active layer. The Pt/active layer/glass structure is diced as an 8 mm wide and 2.54 mm long glass beam, and then it is sandwiched by other glass substrate with epoxy (Epo-Tech 353ND consisting of bisphenol F and imidazole; Epoxy Technology). Two aluminum taps are attached at the specimen to apply loading and delaminate the DCB specimen. The high-precision DCB testing equipment (Delaminator Adhesion Test System; DTS Company, Menlo Park, CA, USA) consists of a linear actuator, and a load cell is used for the adhesion measurement test. All tests are performed in controlled lab air conditions (∼20% RH) at 21 °C, and multiple loading/crack-growth/unloading cycles are performed to measure the adhesion energy. G_c was calculated as the critical value of the strain energy release rate, as in the previous reports.[18,62]

Pseudo Free-Standing Tensile Test. For the tensile testing specimen, the active layers were spin-coated on the PEDOT:PSS/glass substrate. The dog-bone-shaped active layer specimen is prepared by using a cutting plotter (GCC Jaguar IV-61, USA). In order to float the specimen on the water surface, water is penetrated into the PEDOT:PSS layer. Subsequently, PEDOT:PSS is dissolved and the active layer can be delaminated from the glass substrate. By performing this process at the water surface, the floating active layer specimen can be obtained. Specimen gripping is achieved by attaching PDMS-coated Al grips on the specimen gripping areas using van der Waals adhesion. The tensile test is performed by a linear stage with a strain rate of 0.06×10^{-3}/s. During the tensile test, stress and strain data are obtained through a load cell and a DIC device, respectively.

Coarse-Grained Bead-Spring Molecular Dynamics Simulations. The detailed procedures of the molecular dynamics simulation are described in the Supporting Information.

Conflict of Interest: The authors declare no competing financial interest.

Supporting Information Available: Detailed experimental procedure and additional characterization data. This material is available free of charge via the Internet at http://pubs.acs.org.

Acknowledgment. This research was supported by the National Research Foundation Grant (2013R1A2A1A03069803) and by the Global Frontier R&D Program of Center for Multiscale Energy System (2012M3A6A7055540) funded by the Korean Government. This research was supported by the New & Renewable Energy Program of KETEP Grant (20133030011330), funded by the Ministry of Trade, Industry & Energy, Republic of Korea. This research was also supported by the Research Projects of the KAIST-KUSTAR and the KAIST EEWS Initiative (EEWSN01140052). Experiments at PLS were supported in part by MEST and POSTECH.

REFERENCES AND NOTES

1. Krebs, F. C.; Espinosa, N.; Hösel, M.; Søndergaard, R. R.; Jørgensen, M. 25th Anniversary Article: Rise to Power - OPV-Based Solar Parks. *Adv. Mater.* **2014**, *26*, 29–39.
2. Beaujuge, P. M.; Fréchet, J. M. J. Molecular Design and Ordering Effects in π-Functional Materials for Transistor and Solar Cell Applications. *J. Am. Chem. Soc.* **2011**, *133*, 20009–20029.
3. Mei, J.; Bao, Z. Side Chain Engineering in Solution-Processable Conjugated Polymers. *Chem. Mater.* **2013**, *26*, 604–615.
4. Søndergaard, R.; Hösel, M.; Angmo, D.; Larsen-Olsen, T. T.; Krebs, F. C. Roll-to-Roll Fabrication of Polymer Solar Cells. *Mater. Today* **2012**, *15*, 36–49.
5. Dou, L.; You, J.; Hong, Z.; Xu, Z.; Li, G.; Street, R. A.; Yang, Y. 25th Anniversary Article: A Decade of Organic/Polymeric Photovoltaic Research. *Adv. Mater.* **2013**, *25*, 6642–6671.
6. Kang, T. E.; Kim, K.-H.; Kim, B. J. Design of Terpolymers as Electron Donors for Highly Efficient Polymer Solar Cells. *J. Mater. Chem. A* **2014**, *2*, 15252–15267.

7. Rogers, J. T.; Schmidt, K.; Toney, M. F.; Kramer, E. J.; Bazan, G. C. Structural Order in Bulk Heterojunction Films Prepared with Solvent Additives. *Adv. Mater.* **2011**, *23*, 2284–2288.
8. Li, G.; Shrotriya, V.; Huang, J.; Yao, Y.; Moriarty, T.; Emery, K.; Yang, Y. High-Efficiency Solution Processable Polymer Photovoltaic Cells by Self-Organization of Polymer Blends. *Nat. Mater.* **2005**, *4*, 864–868.
9. Ma, W.; Yang, C.; Gong, X.; Lee, K.; Heeger, A. J. Thermally Stable, Efficient Polymer Solar Cells with Nanoscale Control of the Interpenetrating Network Morphology. *Adv. Funct. Mater.* **2005**, *15*, 1617–1622.
10. Li, G.; Zhu, R.; Yang, Y. Polymer Solar Cells. *Nat. Photonics* **2012**, *6*, 153–161.
11. You, J.; Dou, L.; Yoshimura, K.; Kato, T.; Ohya, K.; Moriarty, T.; Emery, K.; Chen, C.-C.; Gao, J.; *et al.* A Polymer Tandem Solar Cell with 10.6% Power Conversion Efficiency. *Nat. Commun.* **2013**, *4*, 1446.
12. Jørgensen, M.; Norrman, K.; Gevorgyan, S. A.; Tromholt, T.; Andreasen, B.; Krebs, F. C. Stability of Polymer Solar Cells. *Adv. Mater.* **2012**, *24*, 580–612.
13. Lee, J. U.; Jung, J. W.; Jo, J. W.; Jo, W. H. Degradation and Stability of Polymer-Based Solar Cells. *J. Mater. Chem.* **2012**, *22*, 24265–24283.
14. Kim, B. J.; Miyamoto, Y.; Ma, B.; Fréchet, J. M. J. Photocrosslinkable Polythiophenes for Efficient, Thermally Stable, Organic Photovoltaics. *Adv. Funct. Mater.* **2009**, *19*, 2273–2281.
15. Cheng, Y.-J.; Hsieh, C.-H.; Li, P.-J.; Hsu, C.-S. Morphological Stabilization by *in-Situ* Polymerization of Fullerene Derivatives Leading to Efficient, Thermally Stable Organic Photovoltaics. *Adv. Funct. Mater.* **2011**, *21*, 1723–1732.
16. Woo, C. H.; Thompson, B. C.; Kim, B. J.; Toney, M. F.; Fréchet, J. M. J. The Influence of Poly(3-hexylthiophene) Regioregularity on Fullerene-Composite Solar Cell Performance. *J. Am. Chem. Soc.* **2008**, *130*, 16324–16329.
17. Lipomi, D. J.; Chong, H.; Vosgueritchian, M.; Mei, J.; Bao, Z. Toward Mechanically Robust and Intrinsically Stretchable Organic Solar Cells: Evolution of Photovoltaic Properties with Tensile Strain. *Sol. Energy Mater. Sol. Cells* **2012**, *107*, 355–365.
18. Brand, V.; Bruner, C.; Dauskardt, R. H. Cohesion and Device Reliability in Organic Bulk Heterojunction Photovoltaic Cells. *Sol. Energy Mater. Sol. Cells* **2012**, *99*, 182–189.
19. Tahk, D.; Lee, H. H.; Khang, D.-Y. Elastic Moduli of Organic Electronic Materials by the Buckling Method. *Macromolecules* **2009**, *42*, 7079–7083.
20. Savagatrup, S.; Makaram, A. S.; Burke, D. J.; Lipomi, D. J. Mechanical Properties of Conjugated Polymers and Polymer-Fullerene Composites as a Function of Molecular Structure. *Adv. Funct. Mater.* **2013**, *24*, 1169–1181.
21. Kaltenbrunner, M.; White, M. S.; Glowacki, E. D.; Sekitani, T.; Someya, T.; Sariciftci, N. S.; Bauer, S. Ultrathin and Lightweight Organic Solar Cells with High Flexibility. *Nat. Commun.* **2012**, *3*.
22. Kim, B. J.; Kang, H.; Char, K.; Katsov, K.; Fredrickson, G. H.; Kramer, E. J. Interfacial Roughening Induced by the Reaction of End-Functionalized Polymers at a PS/P2VP Interface: Quantitative Analysis by DSIMS. *Macromolecules* **2005**, *38*, 6106–6114.
23. Shull, K. R.; Kramer, E. J.; Hadziioannou, G.; Tang, W. Segregation of Block Copolymers to Interfaces between Immiscible Homopolymers. *Macromolecules* **1990**, *23*, 4780–4787.
24. Char, K.; Brown, H. R.; Deline, V. R. Effects of a Diblock Copolymer on Adhesion between Immiscible Polymers. 2. Polystyrene (PS)-PMMA Copolymer between Poly(Phenylene oxide) (PPO) and PMMA. *Macromolecules* **1993**, *26*, 4164–4171.
25. Brown, H. R. Effect of a Diblock Copolymer on the Adhesion between Incompatible Polymers. *Macromolecules* **1989**, *22*, 2859–2860.
26. Sivula, K.; Ball, Z. T.; Watanabe, N.; Fréchet, J. M. J. Amphiphilic Diblock Copolymer Compatibilizers and Their Effect on the Morphology and Performance of Polythiophene: Fullerene Solar Cells. *Adv. Mater.* **2006**, *18*, 206–210.
27. Miyanishi, S.; Zhang, Y.; Tajima, K.; Hashimoto, K. Fullerene Attached All-Semiconducting Diblock Copolymers for Stable Single-Component Polymer Solar Cells. *Chem. Commun.* **2010**, *46*, 6723–6725.
28. Lee, J. U.; Cirpan, A.; Emrick, T.; Russell, T. P.; Jo, W. H. Synthesis and Photophysical Property of Well-Defined Donor-Acceptor Diblock Copolymer Based on Regioregular Poly(3-hexylthiophene) and Fullerene. *J. Mater. Chem.* **2009**, *19*, 1483–1489.
29. Yang, C.; Lee, J. K.; Heeger, A. J.; Wudl, F. Well-Defined Donor-Acceptor Rod-Coil Diblock Copolymers Based on P3ht Containing C_{60}: The Morphology and Role as a Surfactant in Bulk-Heterojunction Solar Cells. *J. Mater. Chem.* **2009**, *19*, 5416–5423.
30. Rajaram, S.; Armstrong, P. B.; Kim, B. J.; Fréchet, J. M. J. Effect of Addition of a Diblock Copolymer on Blend Morphology and Performance of Poly(3-hexylthiophene):Perylene Diimide Solar Cells. *Chem. Mater.* **2009**, *21*, 1775–1777.
31. Sommer, M.; Hüttner, S.; Steiner, U.; Thelakkat, M. Influence of Molecular Weight on the Solar Cell Performance of Double-Crystalline Donor-Acceptor Block Copolymers. *Appl. Phys. Lett.* **2009**, *95*, 183308.
32. Lai, Y.-C.; Higashihara, T.; Hsu, J.-C.; Ueda, M.; Chen, W.-C. Enhancement of Power Conversion Efficiency and Long-Term Stability of P3HT/PCBM Solar Cells Using C_{60} Derivatives with Thiophene Units as Surfactants. *Sol. Energy Mater. Sol. Cells* **2012**, *97*, 164–170.
33. Kim, J. B.; Allen, K.; Oh, S. J.; Lee, S.; Toney, M. F.; Kim, Y. S.; Kagan, C. R.; Nuckolls, C.; Loo, Y.-L. Small-Molecule Thiophene-C_{60} Dyads as Compatibilizers in Inverted Polymer Solar Cells. *Chem. Mater.* **2010**, *22*, 5762–5773.
34. Richards, J. J.; Rice, A. H.; Nelson, R. D.; Kim, F. S.; Jenekhe, S. A.; Luscombe, C. K.; Pozzo, D. C. Modification of Pcbm Crystallization *via* Incorporation of C_{60} in Polymer/Fullerene Solar Cells. *Adv. Funct. Mater.* **2013**, *23*, 514–522.
35. Lee, J. U.; Jung, J. W.; Emrick, T.; Russell, T. P.; Jo, W. H. Synthesis of C_{60}-End Capped P3HT and Its Application for High Performance of P3HT/PCBM Bulk Heterojunction Solar Cells. *J. Mater. Chem.* **2010**, *20*, 3287–3294.
36. Kim, H. J.; Han, A. R.; Cho, C.-H.; Kang, H.; Cho, H.-H.; Lee, M. Y.; Fréchet, J. M. J.; Oh, J. H.; Kim, B. J. Solvent-Resistant Organic Transistors and Thermally Stable Organic Photovoltaics Based on Cross-Linkable Conjugated Polymers. *Chem. Mater.* **2011**, *24*, 215–221.
37. Kang, H.; Cho, C.-H.; Cho, H.-H.; Kang, T. E.; Kim, H. J.; Kim, K.-H.; Yoon, S. C.; Kim, B. J. Controlling Number of Indene Solubilizing Groups in Multiadduct Fullerenes for Tuning Optoelectronic Properties and Open-Circuit Voltage in Organic Solar Cells. *ACS Appl. Mater. Interfaces* **2011**, *4*, 110–116.
38. Lim, J.; Yang, H.; Paek, K.; Cho, C. H.; Kim, S.; Bang, J.; Kim, B. J. "Click" Synthesis of Thermally Stable Au Nanoparticles with Highly Grafted Polymer Shell and Control of Their Behavior in Polymer Matrix. *J. Polym. Sci., Part A: Polym. Chem.* **2011**, *49*, 3464–3474.
39. Kang, H.; Kim, K.-H.; Kang, T. E.; Cho, C.-H.; Park, S.; Yoon, S. C.; Kim, B. J. Effect of Fullerene Tris-Adducts on the Photovoltaic Performance of P3HT:Fullerene Ternary Blends. *ACS Appl. Mater. Interfaces* **2013**, *5*, 4401–4408.
40. Zhao, G.; He, Y.; Li, Y. 6.5% Efficiency of Polymer Solar Cells Based on Poly(3-hexylthiophene) and Indene-C_{60} Bisadduct by Device Optimization. *Adv. Mater.* **2010**, *22*, 4355–4358.
41. He, Y.; Chen, H.-Y.; Hou, J.; Li, Y. Indene-C_{60} Bisadduct: A New Acceptor for High-Performance Polymer Solar Cells. *J. Am. Chem. Soc.* **2010**, *132*, 1377–1382.
42. Kim, K.-H.; Kang, H.; Nam, S. Y.; Jung, J.; Kim, P. S.; Cho, C.-H.; Lee, C.; Yoon, S. C.; Kim, B. J. Facile Synthesis of O-Xylenyl Fullerene Multiadducts for High Open Circuit Voltage and Efficient Polymer Solar Cells. *Chem. Mater.* **2011**, *23*, 5090–5095.
43. Lenes, M.; Wetzelaer, G.-J. A. H.; Kooistra, F. B.; Veenstra, S. C.; Hummelen, J. C.; Blom, P. W. M. Fullerene Bisadducts for Enhanced Open-Circuit Voltages and Efficiencies in Polymer Solar Cells. *Adv. Mater.* **2008**, *20*, 2116–2119.

44. Laiho, A.; Ras, R. H. A.; Valkama, S.; Ruokolainen, J.; Österbacka, R.; Ikkala, O. Control of Self-Assembly by Charge-Transfer Complexation between C_{60} Fullerene and Electron Donating Units of Block Copolymers. *Macromolecules* **2006**, *39*, 7648–7653.
45. Gernigon, V.; Lévêque, P.; Richard, F.; Leclerc, N.; Brochon, C.; Braun, C. H.; Ludwigs, S.; Anokhin, D. V.; Ivanov, D. A.; *et al*. Microstructure and Optoelectronic Properties of P3HT-*b*-P4VP/PCBM Blends: Impact of PCBM on the Copolymer Self-Assembly. *Macromolecules* **2013**, *46*, 8824–8831.
46. Lai, Y. C.; Ohshimizu, K.; Takahashi, A.; Hsu, J. C.; Higashihara, T.; Ueda, M.; Chen, W. C. Synthesis of All-Conjugated Poly(3-hexylthiophene)-*b*-Poly(3-(4′-(3″,7″-dimethyloctyloxy)-3′-pyridinyl)thiophene) and Its Blend for Photovoltaic Applications. *J. Polym. Sci., Part A: Polym. Chem.* **2011**, *49*, 2577–2587.
47. Sary, N.; Richard, F.; Brochon, C.; Leclerc, N.; Lévêque, P.; Audinot, J.-N.; Berson, S.; Heiser, T.; Hadziioannou, G.; *et al*. A New Supramolecular Route for Using Rod-Coil Block Copolymers in Photovoltaic Applications. *Adv. Mater.* **2010**, *22*, 763–768.
48. Renaud, C.; Mougnier, S.-J.; Pavlopoulou, E.; Brochon, C.; Fleury, G.; Deribew, D.; Portale, G.; Cloutet, E.; Chambon, S.; *et al*. Block Copolymer as a Nanostructuring Agent for High-Efficiency and Annealing-Free Bulk Heterojunction Organic Solar Cells. *Adv. Mater.* **2012**, *24*, 2196–2201.
49. Sun, Z.; Xiao, K.; Keum, J. K.; Yu, X.; Hong, K.; Browning, J.; Ivanov, I. N.; Chen, J.; Alonzo, J.; *et al*. PS-*b*-P3HT Copolymers as P3HT/PCBM Interfacial Compatibilizers for High Efficiency Photovoltaics. *Adv. Mater.* **2011**, *23*, 5529–5535.
50. Kim, H. J.; Paek, K.; Yang, H.; Cho, C.-H.; Kim, J.-S.; Lee, W.; Kim, B. J. Molecular Design of "Graft" Assembly for Ordered Microphase Separation of P3HT-Based Rod−Coil Copolymers. *Macromolecules* **2013**, *46*, 8472–8478.
51. Iovu, M. C.; Jeffries-El, M.; Sheina, E. E.; Cooper, J. R.; McCullough, R. D. Regioregular Poly(3-alkylthiophene) Conducting Block Copolymers. *Polymer* **2005**, *46*, 8582–8586.
52. Kamps, A. C.; Fryd, M.; Park, S. J. Hierarchical Self-Assembly of Amphiphilic Semiconducting Polymers into Isolated, Bundled, and Branched Nanofibers. *ACS Nano* **2012**, *6*, 2844–2852.
53. Hau, S. K.; Yip, H. L.; Jen, A. K. Y. A Review on the Development of the Inverted Polymer Solar Cell Architecture. *Polym. Rev.* **2010**, *50*, 474–510.
54. Kim, K.-H.; Kang, H.; Kim, H. J.; Kim, P. S.; Yoon, S. C.; Kim, B. J. Effects of Solubilizing Group Modification in Fullerene Bis-Adducts on Normal and Inverted Type Polymer Solar Cells. *Chem. Mater.* **2012**, *24*, 2373–2381.
55. Kozub, D. R.; Vakhshouri, K.; Orme, L. M.; Wang, C.; Hexemer, A.; Gomez, E. D. Polymer Crystallization of Partially Miscible Polythiophene/Fullerene Mixtures Controls Morphology. *Macromolecules* **2011**, *44*, 5722–5726.
56. Vakhshouri, K.; Kozub, D. R.; Wang, C. C.; Salleo, A.; Gomez, E. D. Effect of Miscibility and Percolation on Electron Transport in Amorphous Poly(3-hexylthiophene)/Phenyl-C_{61}-butyric Acid Methyl Ester Blends. *Phys. Rev. Lett.* **2012**, *108*.
57. Liu, H. W.; Chang, D. Y.; Chiu, W. Y.; Rwei, S. P.; Wang, L. Fullerene Bisadduct as an Effective Phase-Separation Inhibitor in Preparing Poly(3-hexylthiophene)-6,6-phenyl-C_{61}-butyric Acid Methyl Ester Blends with Highly Stable Morphology. *J. Mater. Chem.* **2012**, *22*, 15586–15591.
58. Meng, X.; Zhang, W.; Tan, Z. A.; Li, Y.; Ma, Y.; Wang, T.; Jiang, L.; Shu, C.; Wang, C. Highly Efficient and Thermally Stable Polymer Solar Cells with Dihydronaphthyl-Based [70]-Fullerene Bisadduct Derivative as the Acceptor. *Adv. Funct. Mater.* **2012**, *22*, 2187–2193.
59. Kim, T.-S.; Tsuji, N.; Matsushita, K.; Kobayashi, N.; Chumakov, D.; Geisler, H.; Zschech, E.; Dauskardt, R. H. Tuning Depth Profiles of Organosilicate Films with Ultraviolet Curing. *J. Appl. Phys.* **2008**, *104*, 074113.
60. Lee, C. H.; Kim, J.-H.; Zou, C.; Cho, I. S.; Weisse, J. M.; Nemeth, W.; Wang, Q.; Van Duin, A. C. T.; Kim, T.-S.; *et al*. Peel-and-Stick: Mechanism Study for Efficient Fabrication of Flexible/Transparent Thin-Film Electronics. *Sci. Rep.* **2013**, *3*, 2917.
61. Yoon, T.; Shin, W. C.; Kim, T. Y.; Mun, J. H.; Kim, T.-S.; Cho, B. J. Direct Measurement of Adhesion Energy of Monolayer Graphene as Grown on Copper and Its Application to Renewable Transfer Process. *Nano Lett.* **2012**, *12*, 1448–1452.
62. Bruner, C.; Miller, N. C.; McGehee, M. D.; Dauskardt, R. H. Molecular Intercalation and Cohesion of Organic Bulk Heterojunction Photovoltaic Devices. *Adv. Funct. Mater.* **2013**, *23*, 2863–2871.
63. Dupont, S. R.; Voroshazi, E.; Heremans, P.; Dauskardt, R. H. Adhesion Properties of Inverted Polymer Solarcells: Processing and Film Structure Parameters. *Org. Electron.* **2013**, *14*, 1262–1270.
64. Savagatrup, S.; Makaram, A. S.; Burke, D. J.; Lipomi, D. J. Mechanical Properties of Conjugated Polymers and Polymer-Fullerene Composites as a Function of Molecular Structure. *Adv. Funct. Mater.* **2014**, *24*, 1169–1181.
65. Kim, J.-H.; Nizami, A.; Hwangbo, Y.; Jang, B.; Lee, H.-J.; Woo, C.-S.; Hyun, S.; Kim, T.-S. Tensile Testing of Ultra-Thin Films on Water Surface. *Nat. Commun.* **2013**, *4*, 2520.
66. Savagatrup, S.; Printz, A. D.; Rodriquez, D.; Lipomi, D. J. Best of Both Worlds: Conjugated Polymers Exhibiting Good Photovoltaic Behavior and High Tensile Elasticity. *Macromolecules* **2014**, *47*, 1981–1992.
67. Kim, S. H.; Jo, W. H. A Monte Carlo Simulation of Polymer Polymer Interface in the Presence of Block Copolymer. I. Effects of the Chain Length of Block Copolymer and Interaction Energy. *J. Chem. Phys.* **1999**, *110*, 12193–12201.
68. Zhou, Y.; Long, X.-P.; Zeng, Q.-X. Dissipative Particle Dynamics Studies on the Interface of Incompatible A/B Homopolymer Blends in the Presence of Nanorods. *Polymer* **2011**, *52*, 6110–6116.
69. Irving, J. H.; Kirkwood, J. G. The Statistical Mechanical Theory of Transport Processes. 4. The Equations of Hydrodynamics. *J. Chem. Phys.* **1950**, *18*, 817–829.
70. Hummelen, J. C.; Knight, B. W.; LePeq, F.; Wudl, F.; Yao, J.; Wilkins, C. L. Preparation and Characterization of Fulleroid and Methanofullerene Derivatives. *J. Org. Chem.* **1995**, *60*, 532–538.